THE JOURNAL OF PHYSICAL CHEMISTRY C

Article

pubs.acs.org/JPCC

Micrometer Sized Perovskite Crystals in Planar Hole Conductor Free Solar Cells

Shany Gamliel, Alex Dymshits, Sigalit Aharon, Eyal Terkieltaub, and Lioz Etgar*

Institute of Chemistry, Casali Center for Applied Chemistry, The Hebrew University of Jerusalem, Jerusalem 91904, Israel

Supporting Information

ABSTRACT: In this work we demonstrate the planar configuration on hole conductor (HTM) free perovskite based solar cells. The $CH_3NH_3PbI_3$ perovskite was deposited using the spray technique to achieve micrometer size perovskite crystals. The number of spray passes changes the $CH_3NH_3PbI_3$ film thickness; for example, 10 spray passes achieved a film thickness of 3.4 μm of perovskite. Surprisingly, power conversion efficiency of 6.9% was demonstrated for this novel, simple solar cell structure with thick perovskite film that has no HTM. Capacitance−voltage measurements reveal charge accumulation at the $CH_3NH_3PbI_3$/Au interface while the compact TiO_2/$CH_3NH_3PbI_3$ junction showed a space charge region, which inhibits the recombination. Studying these interfaces is key to understanding the operation mechanism of this unique solar cell structure. This simple planar HTM free perovskite solar cell demonstrates the potential to make large-scale solar cells while maintaining a simple, low-cost architecture.

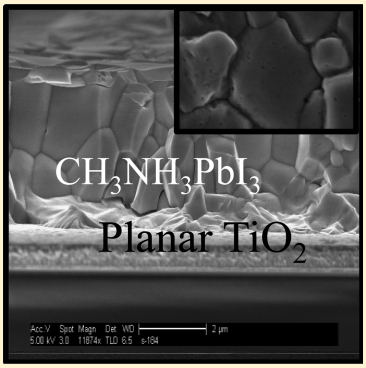

INTRODUCTION

Organometal perovskite is a hybrid material composed of inorganic and organic components having high absorption coefficient, direct band gap, and high carrier mobility,[1−3] making it attractive for photovoltaic (PV) solar cells. In recent years, organometal perovskite has been used intensively in PV solar cells, achieving a power conversion of 20.1%.[4]

Long electron−hole diffusion length was demonstrated in organometal perovskite which contributes to the high power conversion efficiency.[5,6] The perovskite based solar cells are not restricted to a specific solar cell configuration as might occur in other solar cell technologies. It has been demonstrated that perovskite, with and without the ability to inject electrons, functions on mesoporous metal oxide.[7−9] The perovskite can also be used both as a hole conductor (HTM) and as a light harvester due to the efficient hole and electron mobility, making the solar cell structure even simpler. HTM free cells show PV performance of 10−12% efficiency.[10−15] In addition, it is possible to observe efficient perovskite solar cells in planar architecture. In this solar cell structure, the perovskite is usually deposited on a planar substrate, contrary to the mesoporous configuration. One of the first reports on planar architecture discussed the evaporation of the organometal perovskite, achieving a uniform perovskite film with more than 15% efficiency.[16] Moreover, a vapor-assisted solution process was demonstrated as an efficient deposition technique for the planar structure, achieving 12.1% efficiency.[17] Flexible, low temperature planar perovskite solar cells were demonstrated on ZnO nanoparticles exceeding 10% efficiency[18] and on polymer substrate in an inverted configuration, where the perovskite was deposited between PDOT:PSS and PCBM.[19] Recently, inverted planar perovskite based solar cells where a CuSCN layer was deposited on the ITO surface showed 15.6% efficiency. The low interface contact resistance between the perovskite, the CuSCN, and the C60 made possible the high power conversion efficiency.[20] Spray coating of $CH_3NH_3PbI_{3-x}Cl_x$ in a planar structure was studied when the substrate temperature was varied in order to increase the coverage.[21] The ambipolar property of the perovskite was investigated on a planar configuration using linearly increasing voltage (CELIV) and time-of-flight (TOF) revealing balance transport in the perovskite, which helped clarify the operation mechanism of this solar cell.[22] An efficiency of 10% was demonstrated using $CH_3NH_3PbI_2Br$ nanosheets with a 1.8 eV band gap prepared via thermal decomposition in the planar configuration.[23] A recent report showed millimeter scale crystalline grains of perovskite made by the solution hot casting technique, achieving pinhole free film with 18% efficiency.[24] The intensive research work on planar perovskite based solar cells indicates the potential of this solar cell configuration.

In this work, we present a unique planar HTM free perovskite solar cell. The perovskite deposition was done by a facile spray technique to create micrometer sized grains of perovskite film. We used this deposition technique in a simple solar cell configuration consisting of FTO glass/compact TiO_2/$CH_3NH_3PbI_3$/Au. The perovskite functioned both as a light harvester and as a hole conductor in this solar cell structure. The perovskite film thickness and the blocking layer thickness were varied. Interestingly, power conversion efficiency of 6.9% was achieved for the planar HTM free cell with 3.4 μm perovskite film thickness. Capacitance−voltage measurements

Received: August 4, 2015
Published: August 14, 2015

DOI: 10.1021/acs.jpcc.5b07554
J. Phys. Chem. C 2015, 119, 19722−19728

shed more light on the operation mechanism of this unique configuration.

RESULTS AND DISCUSSSION

Figure 1A shows a schematic illustration of the spray deposition technique; the perovskite precursors are sprayed from a one-step solution onto a hot substrate (additional details are found in the Experimental Section). Subsequently, the solvent dimethylformamide (DMF) rapidly evaporates, immediately creating the perovskite crystals. Rapid evaporation of the solvent, which prevents percolation of the perovskite crystals into a mesoporous film, is an important stage of the deposition technique. Low photovoltaic (PV) performance is expected in the case of perovskite cells based on mesoporous metal oxide. Consequently, we used this facile deposition technique for the planar architecture as shown schematically in Figure 1B. The solar cell structure composed of planar anatase TiO_2 film, as confirmed by X-ray diffraction (XRD), shows the anatase XRD peaks in Figure 1C. A thick perovskite film was deposited on the planar TiO_2 by the spray technique, following the evaporation of gold contact. The number of spray passes made over the electrode controlled the thickness of the perovskite film. In this solar cell structure, the perovskite functions as both a light harvester and a hole conductor, which makes this solar cell configuration one of the simplest photovoltaic cell structures.

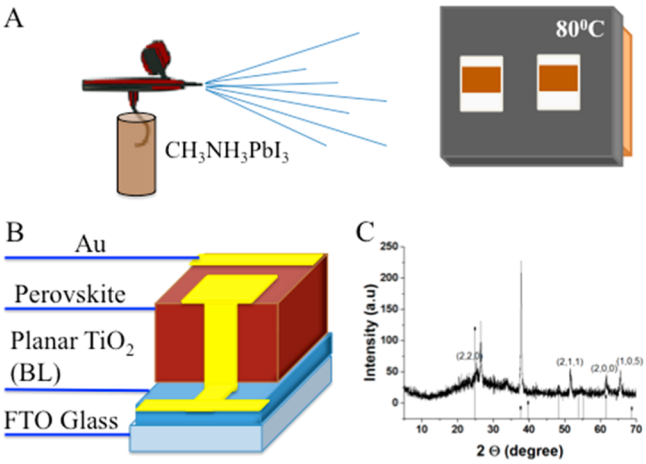

Figure 1. (A) Schematic illustration of the spray deposition technique. (B) Planar HTM free perovskite solar cell structure. (C) XRD of the planar TiO_2 thin film. The anatase TiO_2 crystallographic planes are indexed in the figure.

One of the exceptional properties of this technique is the ability to create thick perovskite films depending on the number of spray passes. A representative absorbance spectrum presented in Figure 2A shows 10 passes of the spray deposition. The onsets of the absorbance spectra show a red shift from the usual absorbance spectra of $CH_3NH_3PbI_3$; this phenomenon was reported earlier by Grancini et al.[25] It was observed that the deposition of $CH_3NH_3PbI_3$ on a flat surface could cause a red shift of the absorption spectra compared to mesoporous film. This red shift is probably due to slow rotation of the methylammonium cation in the flat structure, which screens the excitonic transition at the onset of the absorbance spectra.[25] In addition, an excitonic feature was also observed in the absorbance spectra for the perovskite film deposited on a flat substrate.[26]

Figure 2B shows the XRD of the $CH_3NH_3PbI_3$ perovskite deposited by a two-step deposition technique[12] and by a spray deposition technique. As indicated in Figure 2B, the $CH_3NH_3PbI_3$ peaks are clearly seen; however, two main differences are observed between these deposition techniques. (i) The XRD peaks of the spray deposition technique are much stronger, suggesting thicker film of $CH_3NH_3PbI_3$ observed by the spray technique. (ii) The PbI_2 peak does not appear in the spray deposition technique, in contrast to the two-step deposition, suggesting a complete conversion of the precursors to $CH_3NH_3PbI_3$ perovskite.

Cross-section high-resolution scanning electron microscopy (HR-SEM) images are shown in Figure 3 for the four different perovskite thicknesses made by 4, 6, 8, and 10 spray passes. Figure 3 insets show that the spray deposition technique creates micrometer-sized grains of perovskite depending on the number of spray passes (discussed below in further detail), minimizing the grain boundaries, which is beneficial for the PV performance.

To investigate the PV performance of these cells, the number of blocking layers, i.e., the thickness of the planar TiO_2 films, was changed and the number of passes was varied. Table 1 shows the thickness of the planar TiO_2 film measured by a profilometer. As the number of blocking layers increases, the thickness of the planar TiO_2 also increases. The PV results of cells made on different blocking layers with a constant number of passes (10 passes) are presented in Table 1 and Figure 4A.

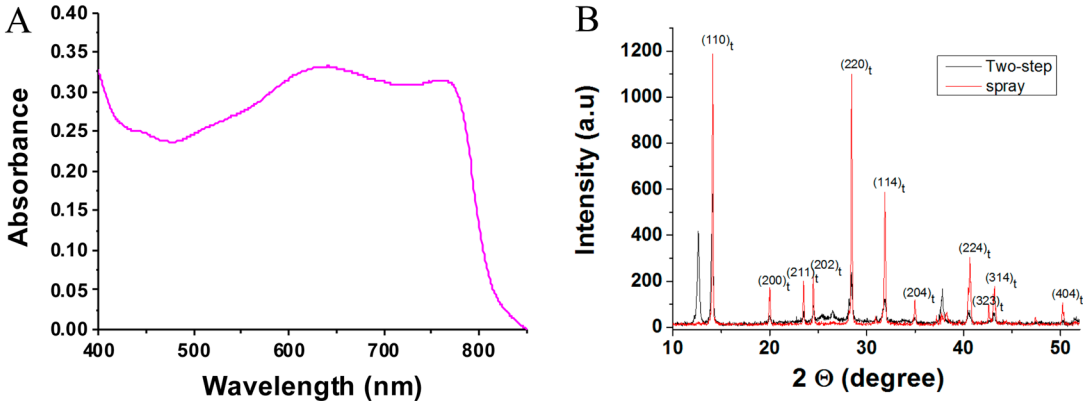

Figure 2. (A) Representative absorbance of 10 spray passes of the $CH_3NH_3PbI_3$ perovskite. (B) XRD of the $CH_3NH_3PbI_3$ made by two-step technique and by spray technique. t, tetragonal.

DOI: 10.1021/acs.jpcc.5b07554
J. Phys. Chem. C 2015, 119, 19722−19728

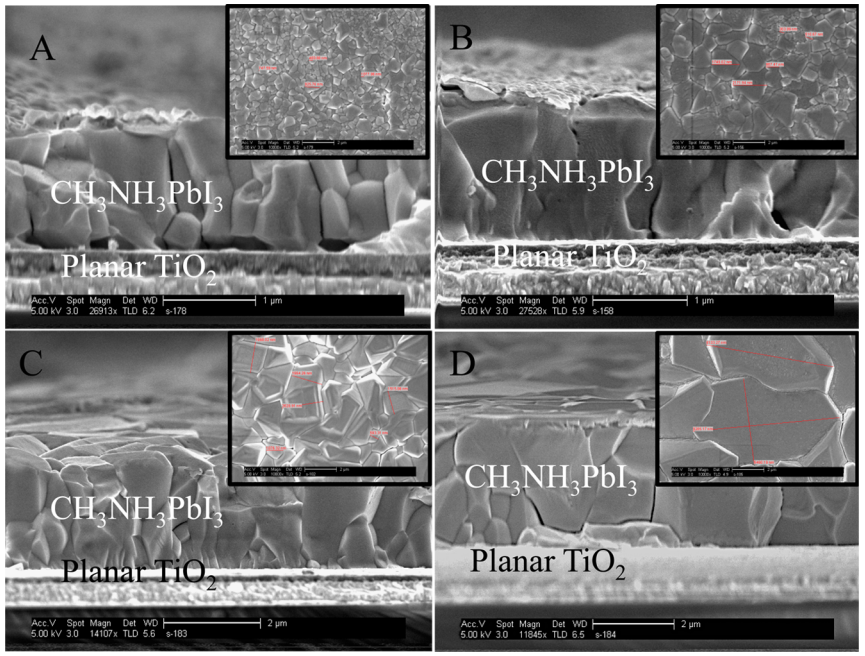

Figure 3. (A) Four passes of perovskite spray; (B) six passes of perovskite spray; (C) eight passes of perovskite spray; (D) 10 passes of perovskite spray. (inset) Top views of different spray passes 4, 6, 8, and 10, respectively. Scale bars in the insets are 2 μm.

Table 1. PV Parameters of Cells According to Various Thicknesses of Dense TiO_2 Layers (Blocking Layers); Thicknesses As Listed in the Table[a]

no. of BL	V_{oc} (V)	J_{sc} (mA/cm^2)	FF (%)	efficiency (%)	BL thickness (nm)
1	0.55	9.35	39	1.99	74.4 ± 11
2	0.66	21.54	32.7	4.63	76.2 ± 15
3	0.69	23.01	43.4	6.93	166.9 ± 19
4	0.65	21.64	39.7	5.58	184.2 ± 13
5	0.68	17.82	42.3	5.11	227.5 ± 42

[a]The number of spray passes is constant, equal to 10. FF, fill factor; BL, blocking layer.

The best PV performance was achieved at 3 blocking layers with open circuit voltage (V_{oc}) of 0.69 V, J_{sc} of 23.01 mA/cm^2, and power conversion efficiency (PCE) of 6.9% (Figure 4B). It can be observed that the V_{oc} barely changed with the change in the blocking layer thickness, (excluding 1 blocking layer, discussed below), which suggests that the main influence on the V_{oc} is the perovskite film thickness (the number of spray passes). The S-shape observed in the *JV* curves of all cells might be related to charge accumulation, discussed below.

The planar HTM free solar cells with 3 blocking layers showed the best PV performance. In the case of 1 and 2 blocking layers, the planar TiO_2 was too thin and some holes in the blocking layer were observed (see Figure S4), which might contribute to the low performance. On the other hand, in the case of 4 and 5 blocking layers, it seems that the planar TiO_2 is too thick for electrons to transport efficiently (also calculated below by the depletion region); therefore, the efficiency decreased.

To optimize the PV performance, the number of passes was changed (while using 3 blocking layers as the planar TiO_2) as shown in Table S1 and Figure 5A. It can be seen that the efficiency is the highest in the case of 10 spray passes as shown in Figure 5B. The reason for the best PV performance in the case of 10 spray passes is mainly due to the difference in the perovskite crystal size. As indicated by the HR-SEM images in

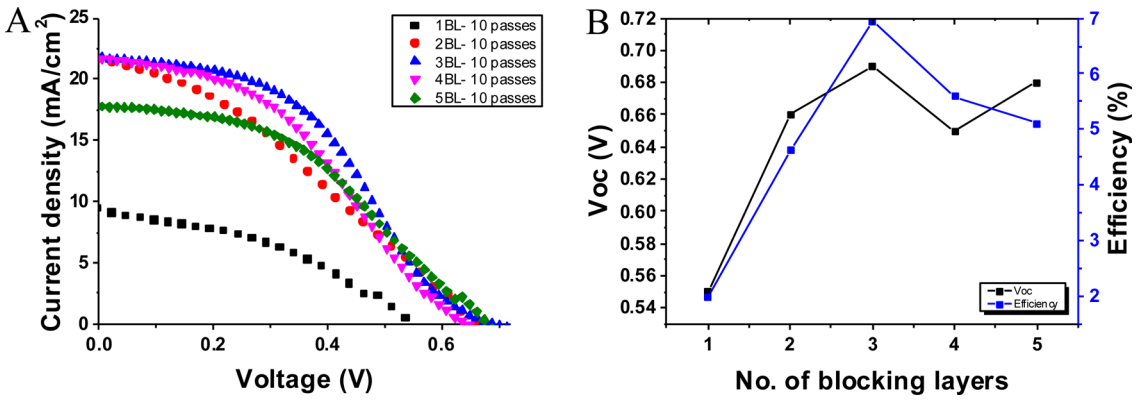

Figure 4. (A) *JV* curves of cells made by 10 passes deposited on various blocking layers. (B) Open circuit voltage and efficiency as a function of the number of blocking layers. BL, blocking layer.

DOI: 10.1021/acs.jpcc.5b07554
J. Phys. Chem. C 2015, 119, 19722−19728

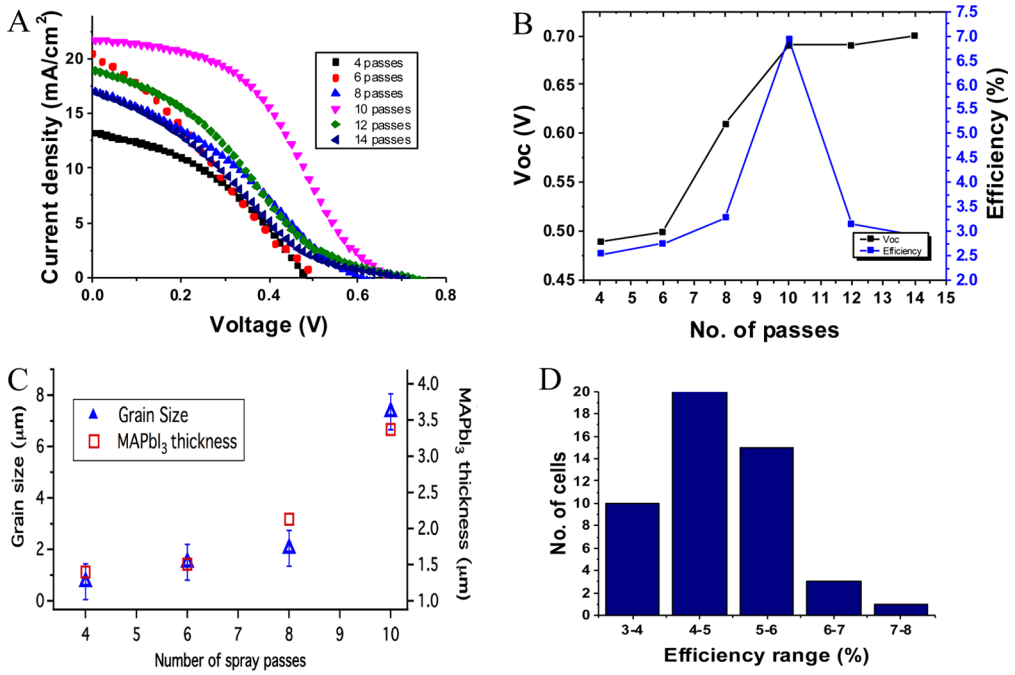

Figure 5. (A) *JV* curves of the cells made on 3 blocking layers according to the number of passes. (B) Open circuit voltage and efficiency as a function of the number of passes. (C) Average grain size and the $MAPbI_3$ film thickness as a function of the number of spray passes. (D) Statistics of the HTM free planar solar cells.

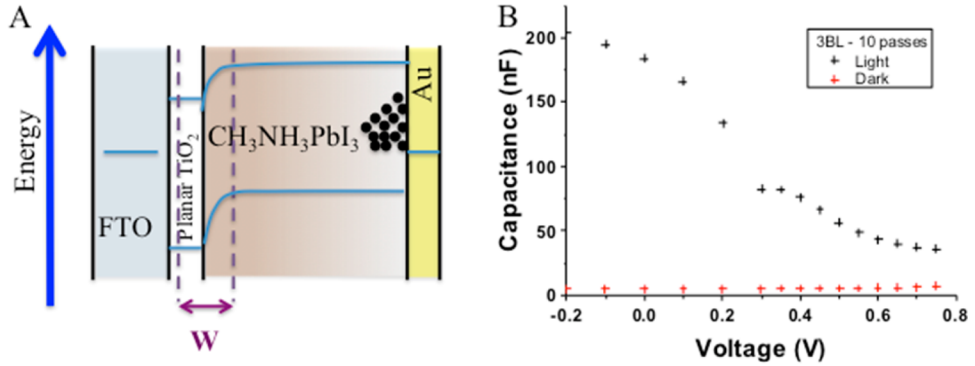

Figure 6. (A) Schematic illustration of the energy level diagram of the planar HTM free perovskite solar cell. (B) Capacitance–voltage measurements in the dark and under illumination of the cell with 3 blocking layers and 10 perovskite spray passes.

Figure 3, the perovskite crystal size increases with the number of spray passes. In the rest of the discussion we excluded 12 and 14 spray passes since the PV performance decreased significantly in these cases (PCE of 3.1 and 2.9% of 12 and 14 spray passes, respectively). The reason for the decrease in performance for the 12 and 14 passes is due to the fact that the perovskite layer becomes very thick and as a result it is peeled from the surface, which harms the PV performance. Figure 5C shows the change in the perovskite crystal size as a function of the number of spray passes. In the case of 10 spray passes the crystal size of the perovskite is 7.5 ± 1 μm (though, a few crystals were smaller than 6.5 μm and some were larger than 8.5 μm). Nie et al.[24] have reported that large perovskite grains have fewer defects and higher mobility enabling better charge carrier transport through the perovskite film. Figure 5A–C supports this argument; the V_{oc} and the efficiency increase with the number of spray passes (bigger perovskite crystals). The increase of the number of spray passes points out the decrease in recombination and defects in the perovskite crystals. Moreover, as indicated by the top view SEM figures (Figure S3 in the Supporting Information), the coverage improved with increasing number of spray passes, further supporting the increase in the efficiency. Figure S5 shows different scan directions and different scan rates in the case of 3 blocking layers with 10 spray passes (the conditions which present the best PV performance); it can be observed that the hysteresis is minimal in these cells and almost independent of the scan rate.

Statistics for the planar HTM free solar cells are presented in Figure 5D. An average efficiency of 4.7 ± 1% was observed for over 50 cells.

To elucidate the mechanism of these planar HTM free perovskite solar cells, capacitance–voltage measurements were performed both in the dark and under illumination. Figure 6B shows the capacitance–voltage measurements for the cell with 3 blocking layers and 10 spray passes of perovskite (this cell demonstrated the best PV performance). All other cells discussed in this paper demonstrated the same capacitance–voltage behavior (see Figures S1 and S2 in the Supporting Information) as the cell shown in Figure 6B. In the dark, the capacitance remained constant at approximately 5×10^{-9} F.

DOI: 10.1021/acs.jpcc.5b07554
J. Phys. Chem. C 2015, 119, 19722–19728

The capacitance under illumination is 2 orders of magnitude larger than the capacitance in the dark. Under illumination, the capacitance started to increase to several orders of magnitude higher than in the dark, approaching the V_{oc} of the cell, implying that photogenerated carriers are accumulated within the solar cell and cannot be effectively collected by the electrode as shown schematically in Figure 6A. (On the other hand, when the capacitance of a solar cell is almost not changing under illumination, photogenerated carriers can be collected effectively by the electrode without charge accumulation.) This observation was also reported by Bisquert et al.,[27] where the increase of the capacitance was measured as a function of the applied voltage for nanostructure cells and planar cells; this was related to charge accumulation in the perovskite which indicates a high density of states (DOS) in the perovskite. Since the perovskite thickness in this planar structure is in the range 1.4−3.4 μm, which is much larger than the perovskite optimum thickness according to its absorption coefficient,[28] carriers are accumulated at the interface with the metal contact (supported by the capacitance−voltage measurements). The accumulation of carriers might be the explanation for the S-shape observed in the *JV* curves of these cells. The S-shaped curves contribute to the low fill factor of the planar HTM free solar cells. It is important to indicate that the observed S-shape was independent of the *JV* scan rate (Figure S5).

From the discussion presented, it could be construed that thinner perovskite film would be beneficial for the planar HTM free cell. According to Table S1 and Figure 5A,B, the PCE at four passes is much lower than the PCE at 10 passes (which produced thicker and larger perovskite crystals as mentioned). Therefore, it could be argued that, besides the charge accumulation at the perovskite/metal interface, there is an additional contribution to the operation mechanism of the planar HTM free cell.

Mott−Schottky analysis[29] was performed on these solar cells to investigate the blocking layer (planar TiO_2)/perovskite interface and to extract the depletion region.

Equation 1 shows the capacitance at the junction, which implies that there are no free carriers at the depletion region.

$$\frac{1}{C^2} = \frac{2}{\varepsilon\varepsilon_0 q A^2 N}(V_{bi} - V) \quad (1)$$

C represents the measured capacitance, *A* is the active area, *V* is the applied bias, ε is the static permittivity, ε_0 is the permittivity of free space, *q* is the elementary charge, and *N* is the doping density of the donor. Using the slope of the Mott−Schottky in the linear region, the depletion region (space charge region) can be extracted. Where the static permittivity of $CH_3NH_3PbI_3$ was measured to be 30,[30,31] the space charge region suppressed the back reaction and inhibits recombination at this interface. The depletion region can be calculated according to eq 2:[32]

$$W_{p,n} = \frac{1}{N_{a,d}}\left(\frac{2\varepsilon V_{bi}}{q\left(\frac{1}{N_a + N_d}\right)}\right)^{1/2} \quad (2)$$

where N_a and N_d are the doping densities of the acceptor and the donor, respectively. Literature values for doping density in anatase TiO_2 start at $N_a = 1 \times 10^{16}$ cm^{-3}.[33−35]

Using eq 2,the depletion region at the planar TiO_2/perovskite junction for 3, 4, and 5 blocking layers was calculated, where W_n is the depletion through the anatase TiO_2 side, W_p is the depletion through the perovskite side, and *W* is the total depletion region. In the cases of 1 and 2 blocking layers the PV performance was low; therefore, the Mott−Schottky analysis was performed for the other blocking layer thicknesses only, while maintaining 10 passes of the perovskite spray. The results are summarized in Table 2.

Table 2. Depletion Region Width versus Number of Blocking Layers at 10 Spray Passes[a]

no. of BL	W_n (nm)	W_p (nm)	*W* (nm)
3	150	117	267
4	112	127	239
5	121	127	238

[a] W_n is the depletion through the anatase TiO_2 side, W_p is the depletion through the perovskite side, and *W* is the total depletion region.

The results showed similar *W* (total depletion region) values for the three cases. The depletion region width for the 3 BL is slightly wider than the others; however, the results for the perovskite films (W_p = 117−127 nm) indicate that most of the perovskite film is not depleted. At illumination close to the junction the carriers—the holes in this case—are transported to the back contact and cross the whole perovskite film. It is possible that the long diffusion length of electrons and holes is not solely responsible for the operation of this planar HTM free cell. It is suggested that, once a charge separation occurs close to the depletion region, electrons drift to the edge of the depletion region (close to the FTO) while holes are transported to the back contact. In the case of thick perovskite film, the holes are transported without any interference through the perovskite film because, far from the depletion region, there are no free electrons and holes that can recombine with the transported holes. On the other hand, if the charge separation occurs far from the planar TiO_2/perovskite junction, a recombination will probably occur, one of the reasons for the low open circuit voltage observed in these cells.

CONCLUSIONS

This work describes a simple solar cell structure, i.e., planar HTM free perovskite solar cells. The perovskite deposition was made by a special spray deposition technique, which enables changing the perovskite thickness. Perovskite thicknesses in the range 1.4−3.4 μm were observed with micrometer-sized perovskite crystals depending on the number of spray passes. The best PV performance was achieved for 3 blocking layers with 10 spray passes having 6.9% efficiency.

Two main contributions to the PV mechanism were analyzed in this device structure. A depletion region was observed at the planar TiO_2/perovskite junction, while charge accumulation was recognized at the perovskite/metal oxide interface.

Surprisingly, this novel, simple device structure with thick perovskite film showed reasonable PV performance even without HTM. Future work, essential to increase the PV performance of these cells, will be the improvement of the charge carrier collection of these simple planar HTM free devices.

EXPERIMENTAL SECTION

Device Fabrication. SnO_2:F(FTO) conducting glass (15 Ω cm^{-1} Pilkington) was etched with zinc powder and HCl (37%)

DOI: 10.1021/acs.jpcc.5b07554
J. Phys. Chem. C 2015, 119, 19722−19728

to obtain the desired electrode pattern. The FTO glass was then washed with methanol, acetone, and deionized water, and finally was sonicated for 15 min. A compact layer of TiO_2 (blocking layer) was then spin-coated on to the FTO substrate using a solution of titanium diisopropoxidebis(acetylacetonate) (TiDIP, 75% in isopropanol, Aldrich) in ethanol and then annealed at 450 °C for 35 min. Various thicknesses of the blocking layer were achieved by repeating this process two, three, four, and five times. Next, the electrode was treated with a 2 M aqueous $TiCl_4$ solution diluted in 150 mL of TDW. A 60 wt % $CH_3NH_3PbI_3$ perovskite solution was prepared by mixing 1 M methylammonium iodide (CH_3NH_3I was synthesized as described earlier[11] with 1 M lead iodide (Sigma-Aldrich 98%) in *N*-dimethylformamide (DMF). The solution was sprayed onto the electrodes at 80 °C and then annealed inside the glovebox at 80 °C for 40 min. Large $CH_3NH_3PbI_3$ crystals formed immediately on the electrode as the DMF evaporated, indicated by the formation of a dark brown color on the electrode. The thickness of the film was controlled by the number of spray passes made over the electrode. Finally, 40 nm of gold back contact was evaporated under 5×10^{-6} Torr. The active area of the cell was 0.04 cm^2.

Profilometer. A Veeco Dektak 150 profiler was used to measure the thickness of the blocking layer.

X-ray Diffraction. X-ray diffraction measurements were performed using the D8 Advance diffractometer (Bruker AXS, Karlsruhe, Germany) with a secondary graphite monochromator, 2° Soller slits, and a 0.2 mm receiving slit. XRD patterns within the range 5−60° 2θ were recorded at room temperature using Cu Kα radiation (λ = 1.5418 Å) with the following measurement conditions: a tube voltage of 40 kV, a tube current of 40 mA, step-scan mode with a step size of 0.02° 2θ, and a counting time of 1−3 s per step. At the GIXRD (grazing incidence X-ray diffraction), the value of the grazing incidence angle was 2.5°.

Ultra High Resolution Scanning Electron Microscopy (UHR-SEM). A Magellan UHR SEM of FEI (Field Emission Instruments, The Netherlands) was used to obtain the images. The conditions measurements were at 5 kV at various magnifications.

Capacitance−Voltage. Measurements were performed using a Metrohm Autolab system, equipped with a PGTSTAT302N potentiostat instrument. The frequency was 1 kHz at bias potentials between 0 and 0.8 V.

Absorbance. The absorbance measurements were performed on a Jasco V-670. Sample absorption was measured without the gold contact.

Photovoltaic Characterization. Photovoltaic measurements were made using a New Port system, an Oriel *I*−*V* test station with an Oriel Sol3A simulator. The solar simulator is class AAA for spectral performance, uniformity of irradiance, and temporal stability. The solar simulator is equipped with a 450 W xenon lamp. The output power is adjusted to match AM 1.5 global sunlight (100 mW cm^{-2}). The spectral match classifications are IEC 60904-9 2007, JIC C 8912, and ASTM E927-05. *I*−*V* curves were obtained by applying an external bias to the cell and measuring the generated photocurrent with a Keithley Model 2400 digital source meter. The voltage step and delay time of photocurrent were 10 mV and 40 ms, respectively. Photovoltaic performance was measured by using a metal mask with an aperture area of 0.04 cm^2.

■ ASSOCIATED CONTENT

Supporting Information

The Supporting Information is available free of charge on the ACS Publications website at DOI: 10.1021/acs.jpcc.5b07554.

Capacitance voltage measurements in the dark and under light; SEM images of different spray passes; SEM images of blocking layers deposited on FTO; scan rates of forward to reverse and reverse to forward of the best conditions for the planar structure; PV parameters of cells made on the blocking layers according to number of passes (PDF)

■ AUTHOR INFORMATION

Corresponding Author

*E-mail: lioz.etgar@mail.huji.ac.il.

Notes

The authors declare no competing financial interest.

■ ACKNOWLEDGMENTS

We are grateful for the financial support of the Israel Alternative Energy Foundation (I-SAEF), the Ministry of Industry Trade and Labor Office of the Chief Scientist Kamin Project No. 50303, the Tashtiot project of the Office of the Chief Scientist, and the German Israel Foundation for young researchers.

■ REFERENCES

(1) Kojima, A.; Ikegami, M.; Teshima, K.; Miyasaka, T. Highly Luminescent Lead Bromide Perovskite Nanoparticles Synthesized with Porous Alumina Media. *Chem. Lett.* **2012**, *41*, 397−399.

(2) Kagan, C. R.; Mitzi, D. B.; Dimitrakopoulos, C. D. Organic-Inorganic Hybrid Materials as Semiconducting Channels in Thin-Film Field-Effect Transistors. *Science* **1999**, *286*, 945−947.

(3) Mitzi, B. D.; Feild, A. C.; Schlesinger, Z.; Laibowitz, B. R. Transport Optical and Magnetic properties of the conducting Halide Perovskite $CH_3NH_3SnI_3$. *J. Solid State Chem.* **1995**, *114*, 159−163.

(4) http://www.nrel.gov/ncpv/images/efficiency_chart.jpg.

(5) Stranks, D. S.; Eperon, E. G.; Grancini, G.; Menelaou, C.; Alcocer, J. P.M; Leijtens, T.; Herz, M. L.; Petrozza, A.; Snaith, J. H. Electron-Hole Diffusion Lengths Exceeding 1 Micrometer in an Organo metal Trihalide Perovskite Absorber. *Science* **2013**, *342*, 341−344.

(6) Xing, G.; Mathews, N.; Sun, G. S.; Lim, S. S.; Lam, M. Y.; Grätzel, M.; Mhaisalkar, S.; Sum, C. T. Long-Range Balanced Electron- and Hole-Transport Lengths in Organic-Inorganic $CH_3NH_3PbI_3$. *Science* **2013**, *342*, 344−347.

(7) Lee, M. M.; Teuscher, M. J.; Miyasaka, T.; Murakami, T. N.; Snaith, H. J. Efficient Hybrid Solar Cells Based on Meso-Superstructured Organometal Halide Perovskites. *Science* **2012**, *338*, 643−644.

(8) Ball, M. J.; Lee, M. M.; Hey, A.; Snaith, J. H. Low-temperature processed meso-superstructured to thin-film perovskite solar cells. *Energy Environ. Sci.* **2013**, *6*, 1739−1743.

(9) Heo, J. H.; Im, S. H.; Noh, J. H.; Mandal, T. N.; Lim, C.-S.; Chang, J. A.; Lee, Y. H.; Kim, H. J.; Sarkar, A.; Nazeeruddin, Md. K.; Grätzel, M.; Seok, S. I. Efficient inorganic−organic hybrid heterojunction solar cells containing perovskite compound and polymeric hole conductors. *Nat. Photonics* **2013**, *7*, 486−491.

(10) Laban, W. A.; Etgar, L. Depleted hole conductor-free lead halide iodide heterojunction solar cells. *Energy Environ. Sci.* **2013**, *6*, 3249−3253.

(11) Aharon, S.; Cohen, B. E.; Etgar, L. Hybrid Lead Halide Iodide and Lead Halide Bromide in Efficient Hole Conductor Free Perovskite Solar Cell. *J. Phys. Chem. C* **2014**, *118*, 17160−17165.

DOI: 10.1021/acs.jpcc.5b07554
J. Phys. Chem. C 2015, 119, 19722−19728

(12) Cohen, B. E.; Gamliel, S.; Etgar, L. Parameters influencing the deposition of methylammonium lead halide iodide in hole conductor free perovskite-based solar cells. *APL Mater.* **2014**, *2*, 081502.
(13) Shi, J.; Dong, J.; Lv, S.; Xu, Y.; Zhu, L.; Xiao, J.; Xu, X.; Wu, H.; Li, D.; Luo, Y.; Meng, Q. Hole-conductor-free perovskite organic lead iodide heterojunction thin-film solar cells: High efficiency and junction property. *Appl. Phys. Lett.* **2014**, *104*, 063901.
(14) Aharon, S.; Gamliel, S.; Cohen, B. E.; Etgar, L. Depletion region effect of highly efficient hole conductor free CH3NH3PbI3 perovskite solar cells. *Phys. Chem. Chem. Phys.* **2014**, *16*, 10512−10518.
(15) Mei, A.; Li, X.; Liu, L.; Ku, Z.; Liu, T.; Rong, Y.; Xu, M.; Hu, M.; Chen, J.; Yang, Y.; Grätzel, M.; Han, H. A hole-conductor-free, fully printable mesoscopic perovskite solar cell with high stability. *Science* **2014**, *345*, 295−298.
(16) Liu, M.; Johnston, B. M.; Snaith, J. H. Efficient planar heterojunction perovskite solar cells by vapour deposition. *Nature* **2013**, *501*, 395−398.
(17) Chen, Q.; Zhou, H.; Hong, Z.; Luo, S.; Duan, H. S.; Wang, H. H.; Liu, Y.; Li, G.; Yang, Y. Planar Heterojunction Perovskite Solar Cells via Vapor-Assisted Solution Process. *J. Am. Chem. Soc.* **2014**, *136*, 622−625.
(18) Liu, D.; Kelly, T. L. Perovskite solar cells with a planar heterojunction structure prepared using room-temperature solution processing techniques. *Nat. Photonics* **2014**, *8*, 133−138.
(19) Docampo, P.; Ball, M. J.; Darwich, M.; Eperon, E. G.; Snaith, J. H. Efficient organo metal trihalide perovskite planar-heterojunction solar cells on flexible polymer substrates. *Nat. Commun.* **2013**, *4*, 2761.
(20) Ye, S.; Sun, W.; Li, Y.; Yan, W.; Peng, H.; Bian, Z.; Liu, Z.; Huang, C. CuSCN-Based Inverted Planar Perovskite Solar Cell with an Average PCE of 15.6%. *Nano Lett.* **2015**, *15*, 3723−3728.
(21) Barrows, A. T.; Pearson, A. J.; Kwak, C. K.; Dunbar, A. D. F.; Buckley, A. R.; Lidzey, D. G. Efficient planar heterojunction mixed-halide perovskite solar cells deposited via spray- deposition. *Energy Environ. Sci.* **2014**, *7*, 2944−2950.
(22) Chen, Y.; Peng, J.; Su, D.; Chen, X.; Liang, Z. Efficient and Balanced Charge Transport Revealed in Planar Perovskite Solar Cells. *ACS Appl. Mater. Interfaces* **2015**, *7*, 4471−4475.
(23) Zhao, Y.; Zhu, K. Efficient Planar Perovskite Solar Cells Based on 1.8 eV Band Gap CH3NH3PbI2Br Nanosheets via Thermal Decomposition. *J. Am. Chem. Soc.* **2014**, *136*, 12241−12244.
(24) Nie, W.; Tsai, H.; Asadpour, R.; Blancon, J. C.; Neukirch, A. J.; Gupta, G.; Crochet, J. J.; Chhowalla, M.; Tretiak, S.; Alam, M. A.; Wang, H. L.; Mohite, A. D. High-efficiency solution-processed perovskite solar cells with millimeter-scale grains. *Science* **2015**, *347*, 522−525.
(25) Grancini, G.; Marras, S.; Prato, M.; Giannini, C.; Quarti, C.; De Angelis, F.; De Bastiani, M.; Eperon, E. G.; Snaith, J. H.; Manna, L.; Petrozza, A. The Impact of the Crystallization Processes on the Structural and Optical Properties of Hybrid Perovskite Films for Photovoltaics. *J. Phys. Chem. Lett.* **2014**, *5*, 3836−3842.
(26) D'Innocenzo, V.; Grancini, G.; Alcocer, M. J. P.; Kandada, A. R. S.; Stranks, S. D.; Lee, M. M.; Lanzani, G.; Snaith, H. J.; Petrozza, A. Excitons versus Free Charges in Organo-Lead Tri-halide Perovskites. *Nat. Commun.* **2014**, *5*, 3586.
(27) Kim, H.-S.; Mora-Sero, I.; Gonzalez-Pedro, V.; Fabregat-Santiago, F.; Juarez-Perez, E. J.; Park, N.-G.; Bisquert, J. Mechanism of carrier accumulation in perovskite thin-absorber solar cells. *Nat. Commun.* **2013**, *4*, 2242.
(28) De Wolf, S.; Holovsky, J.; Moon, S. J.; Löper, P.; Niesen, B.; Ledinsky, M.; Haug, F.-J.; Yum, J.-H.; Ballif, C. Organometallic Halide Perovskites: Sharp Optical Absorption Edge and Its Relation to Photovoltaic Performance. *J. Phys. Chem. Lett.* **2014**, *5*, 1035−1039.
(29) Schottky, W. Vereinfachte und Erweiterte Theorie der Randschicht-Gleichrichter. *Eur. Phys. J. A* **1942**, *118*, 539−592.
(30) Poglitsch, A.; Weber, D. Dynamic disorder in methylammonium trihalogeno plumbates (II) observed by millimeter wave spectroscopy. *J. Chem. Phys.* **1987**, *87*, 6373−6378.
(31) Baikie, T.; Fang, Y.; Kadro, J. M.; Schreyer, M.; Wei, F.; Mhaisalkar, S. G.; Graetzel, M.; White, T. J. Synthesis and crystal chemistry of the hybrid perovskite $(CH_3NH_3)PbI_3$ for solid-state sensitized solar cell applications. *J. Mater. Chem. A* **2013**, *1*, 5628−5641.
(32) Luther, M. J.; Law, M.; Beard, C. M.; Song, Q.; Reese, O. M.; Ellingson, J. R.; Nozik, J. A. Schottky Solar Cells Based on Colloidal Nanocrystal Films. *Nano Lett.* **2008**, *8*, 3488−3492.
(33) O'Regan, B.; Moser, J.; Anderson, M.; Graetzel, M. Vectorial electron injection into transparent semiconductor membranes and electric field effects on the dynamics of light-induced charge separation. *J. Phys. Chem.* **1990**, *94*, 8720−8726.
(34) Nakade, S.; Saito, Y.; Kubo, W.; Kanzaki, T.; Kitamura, T.; Wada, Y.; Yanagida, S. Enhancement of electron transport in nano-porous TiO_2 electrodes by dye adsorption. *Electrochem. Commun.* **2003**, *5*, 804−808.
(35) Zaban, A.; Meier, A.; Gregg, B. A. Electric Potential Distribution and Short-Range Screening in Nanoporous TiO_2 Electrodes. *J. Phys. Chem. B* **1997**, *101*, 7985−7990.

DOI: 10.1021/acs.jpcc.5b07554
J. Phys. Chem. C 2015, 119, 19722−19728